

# METAL-DIELECTRIC PHASE TRANSITION OF VO<sub>2</sub> ASSISTED BROADBAND AND HIGH-EFFICIENCY BIFUNCTIONAL METASURFACE IN THE TERAHERTZ FREQUENCY

Nguyen Thi Minh<sup>1,3</sup>, Nguyen Thi Kim Thu<sup>1,3</sup>, Nguyen Thi Hong Van<sup>1</sup>,  
Nguyen Thi Minh Tam<sup>1</sup>, Ho Thi Huyen Thuong<sup>1</sup>, Phan Duy Tung<sup>2</sup>, Vu Dinh Lam<sup>1</sup>,  
Nguyen Thi Quynh Hoa<sup>3,\*</sup>

<sup>1</sup>Graduate University of Science and Technology, Vietnam Academy of Science and Technology, Ha Noi, Viet Nam, 18 Hoang Quoc Viet, Cau Giay, Ha Noi, Viet Nam

<sup>2</sup>Centre for Wireless Communications, University of Oulu. 90570 Oulu, Finland

<sup>3</sup>School of Engineering and Technology, Vinh University, 182 Le Duan, Nghe An, Viet Nam

\*Emails: ntqhoa@vinhuni.edu.vn

Received: 15 April 2022; Accepted for publication: 4 July 2022

**Abstract.** The integration of multiple varied functionalities into a single and compact EM-based device is greatly demanded in EM integration due to their miniaturized configurations. In this paper, a broadband and high-efficiency bifunctional metasurface employing vanadium dioxide (VO<sub>2</sub>) is proposed for the terahertz (THz) frequencies. Due to the dielectric-to-metal transition of VO<sub>2</sub>, the metasurface can be dynamically tuned from a reflecting surface to a broadband absorber under low-temperature conditions. When VO<sub>2</sub> is in the dielectric phase, the designed metasurface shows excellent reflection (> 96 %) in a broad frequency range from 0.5 THz to 4.5 THz. Once VO<sub>2</sub> is heated up and transitioned to its metal phase, the proposed metasurface structure efficiently absorbs normally incident EM waves in the frequency range of 1.29 THz to 3.26 THz with an average absorption of 94.3 %. Moreover, the high absorption characterization of the proposed metasurface is maintained with a wide incident angle and is polarization-insensitive due to its symmetric structure, which makes it suitable for THz applications.

**Keywords:** Vanadium dioxide, metasurface, broadband absorber.

**Classification numbers:** 2.11, 2.2.2, 2.10.1.

## 1. INTRODUCTION

Recently, metasurface, a two-dimensional (2D) metamaterial (MM) type, has attracted interest as it can provide a compact and efficient design solution for electromagnetic (EM)-based devices. Recently, various planar metasurface EM devices with compact size have been demonstrated to exhibit similar functionalities to their bulk counterparts. Therefore, the use of super-thin metasurfaces to manipulate EM waves has been extensively studied including communications [1, 2], sensing [3], imaging [4], and data storage [5, 6]. However, most designs are confined to a mono-functional operation, which significantly hinders the promising application of the metasurface-based EM devices. The tunable and multifunctional metasurfaces

enable to facilitate switchable functionalities and multiple functionalities which are extremely essential and useful for integrated optics and microwaves, well alleviating the aforementioned issues. Therefore, the idea of an EM device that possesses multiple diversified functionalities is greatly desired in EM integration.

Several methods have been reported so far to realize multi-functional metasurface using mechanical actuation [7 - 9], optical [10], electrical [11, 12], or thermal [13 - 24] approaches. In [9], the authors used an origami-based stretchable MM structure to switch between reflector function and absorber function in the microwave frequency band. However, the mechanical method uses an additional bending system to switch metasurface structure to a desired working mode, therefore, it is very difficult to apply this approach to the THz band where the dimensions of unit cells are very small (a few tens of micrometers). For the thermal approach, incorporating conventional metasurfaces with phase-change materials (PCMs) such as vanadium dioxide ( $\text{VO}_2$ ) [13 - 19] or chalcogenide GeSbTe (GST) alloys [20 - 24] is an effective method for the THz band. Under temperature control, PCMs switch between dielectric and metal phases leading to PCM-based metasurfaces that can exhibit multi-functions with a single physical design. Vanadium dioxide is particularly intriguing because it possesses a reversible phase transition at low temperatures, which is essential for obtaining low-power devices. In general, the GST transition threshold temperature is higher, and repeated cycling is limited by deterioration caused by amorphous crystalline phase transitions. The use of PCM can be considered as an effective way to realize multifunctional metasurfaces. Despite the tremendous progresses in PCMs-based metasurfaces with dynamic responses, switchable metasurfaces with several capabilities that can be actively switched over a wide frequency range remain mostly studied.

In this paper, we present a broadband and high-efficiency bifunctional metasurface employing  $\text{VO}_2$  for the applications of terahertz (THz) band. The metasurface structure shows excellent reflection ( $> 96\%$ ) in the dielectric phase of  $\text{VO}_2$  and efficient absorption (above  $90\%$ ) in a wide frequency band when  $\text{VO}_2$  turns to a metal phase. Moreover, the high absorption property of the proposed metasurface is maintained with a wide incident angle and is polarization-insensitive due to its symmetric structure, which makes it suitable for THz applications.

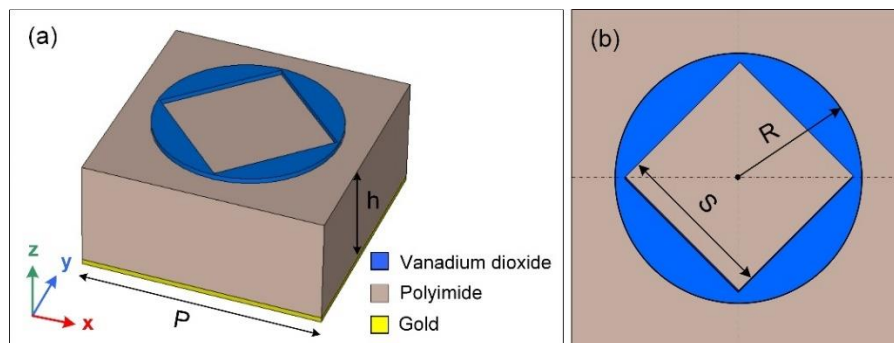


Figure 1. Diagram of a unit cell of the proposed metasurface structure: (a) 3D view and (b) top view.

## 2. STRUCTURE DESIGN AND METHOD

As depicted in Fig. 1, the unit cell of the bifunctional metasurface consists of a  $\text{VO}_2$  pattern on the top layer, acting as a resonator, and a continuous gold sheet at the bottom, acting as a

ground plane. The top layer and bottom layer are separated by a polyimide layer ( $\epsilon=3.5$ ,  $\tan\delta=0.0027$ ). In our simulation, the relative permittivity of VO<sub>2</sub> material is described by Drude model:  $\epsilon(\omega) = \epsilon_\infty - \frac{\omega_p^2(\sigma)}{\omega^2 + i\gamma\omega}$ , with epsilon infinity  $\epsilon_\infty = 12$ , the collision frequency  $\gamma = 5.75 \times 10^{13}$  rad/s, and the plasma frequency can be given by  $\omega_p^2(\sigma) = \frac{\sigma}{\sigma_0} \omega_p^2(\sigma_0)$  with  $\sigma_0 = 3 \times 10^5$  and  $\omega_p(\sigma_0) = 1.4 \times 10^{15}$  rad/s. It is worthy to note that VO<sub>2</sub> is a phase transition material that shows the transition behavior from the insulator phase to the metal phase with increasing temperature above the heating point temperature of 68 °C [14]. The conductivity  $\sigma$  of VO<sub>2</sub> material in the insulator phase and metal phase is 200 S/m and  $2 \times 10^5$  S/m which corresponds to a resistivity of 0.5 Ω.cm and  $0.5 \times 10^{-3}$  Ω.cm, respectively [14].

The absorption performance of the metasurface structure is simulated using CST Microwave Studio 2013. The absorption ( $A(\omega)$ ) of the metasurface structure can be determined from the transmittance ( $T(\omega)$ ), and reflectance ( $R(\omega)$ ), as  $A(\omega) = 1 - R(\omega) - T(\omega)$ . Since the continuous gold layer is thicker than the penetration depth of the THz wave,  $T(\omega)$  can be neglected. Therefore, the absorptance is determined from the reflectance as  $A(\omega) = 1 - R(\omega)$ .

The dimension of the unit cell is tuned to achieve the optimum performance of the proposed bifunctional metasurface structure. The optimum dimensions are listed in Table 1.

Table 1. Optimum parametric value of the proposed bifunctional VO<sub>2</sub> metasurface.

Parameter	<i>P</i>	<i>h</i>	<i>S</i>	<i>R</i>
Value (μm)	38	17	20	16

### 3. ABSORPTION PERFORMANCE AND MECHANISM

Figure 2 shows the absorption spectra of the metasurface structure under different conductivity levels of VO<sub>2</sub>. It is worthy to note that the dielectric and metal phases of VO<sub>2</sub> are assumed to have conductivity of  $2 \times 10^2$  S/m and  $2 \times 10^5$  S/m, respectively. As shown in Fig. 2, when the conductivity changes from  $2 \times 10^2$  S/m to  $2 \times 10^5$  S/m, the absorptance continuously increases from 4 % to 98 %. This phenomenon is mainly attributed to the variation of VO<sub>2</sub> permittivity since the change of the imaginary parts of the permittivity under different conductivity levels is much larger than that of the real part.

With changes in the phase of VO<sub>2</sub> from dielectric to metal, the results in Fig. 2 demonstrate that the proposed metasurface structure can achieve active tunability from wideband reflector to wideband absorber. To further study tunable behavior mechanism of the metasurface structure, the surface electric field distribution at different conductivity levels of VO<sub>2</sub> is simulated as shown in Fig. 3. When the conductivity of VO<sub>2</sub> is low, i.e.  $2 \times 10^2$  S/m, the electric field distributes uniformly on the top layer of the metasurface indicating that VO<sub>2</sub> is transparent to EM waves in the THz band. In this case, most EM waves can penetrate the dielectric layer and reflect back from the ground plane resulting in a low absorption performance as observed in Fig. 2.

With increasing the conductivity from  $2 \times 10^3$  S/m to  $2 \times 10^5$  S/m, VO<sub>2</sub> transforms from the dielectric to the metal phase, which results in the electric field being gradually coupled with the inner edge of the VO<sub>2</sub> pattern. The resonant response of the VO<sub>2</sub> pattern is enhanced and a sharp increase in the absorption performance of the metasurface structure can be observed as in Fig. 2. In addition, the surface electric field distributions at 68 °C (with a conductivity of  $8 \times 10^4$  S/m) and 74

°C (with a conductivity of  $2 \times 10^5$  S/m) are almost the same (not shown here). This is due to the fact that VO<sub>2</sub> is completely transformed into its metal phase at 68 °C. Therefore, the resonant response produced by the VO<sub>2</sub> metasurface structure does not improve as the temperature rises above 68 °C.

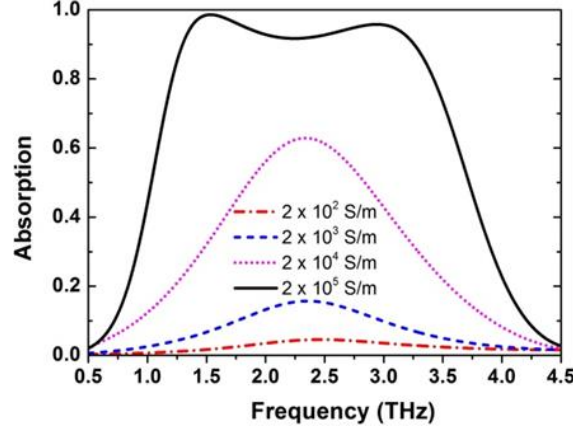


Figure 2. Absorption spectrum of the metasurface structure with different conductivity levels of VO<sub>2</sub>.

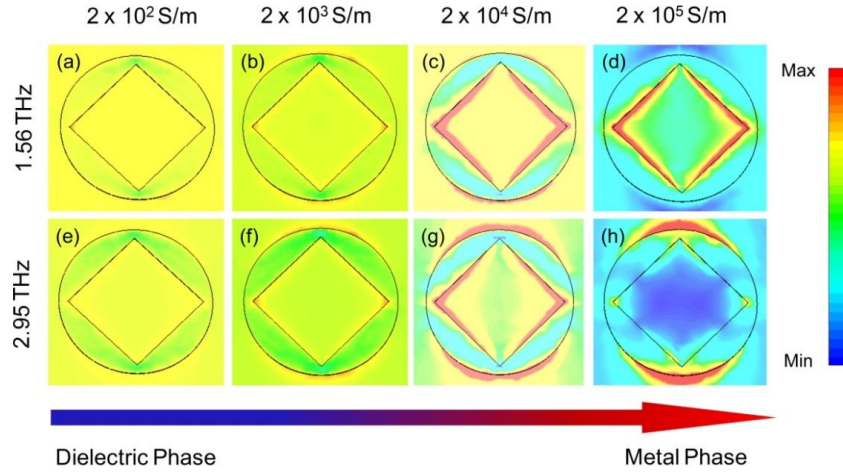


Figure 3. Distribution of the surface electric field at the resonant frequencies corresponds to perfect absorption of 1.56 THz and 2.95 THz and different conductivities of the VO<sub>2</sub>.

The physical mechanism behind the perfect absorption characteristic of the metasurface structure can be explained using the impedance matching theory. As aforementioned, the transmitted EM wave is blocked by the ground plane, therefore, a perfect absorption of the metasurface structure can be achieved by minimizing the reflection. According to the matching theory, the reflection reaches a minimum when the effective impedance of a structure matches that of free space. The absorptance,  $A(\omega)$ , and the relative impedance,  $Z(\omega)$ , can be obtained by Eqs. (1) and (2), respectively.

$$A(\omega) = 1 - R(\omega) = 1 - \left| \frac{Z(\omega) - 1}{Z(\omega) + 1} \right|^2 \quad (1)$$

$$Z(\omega) = \frac{Z_{in}(\omega)}{Z_0} \quad (2)$$

where  $Z_{in}(\omega)$  is the input impedance of the metasurface structure,  $Z_0(\omega)$  is the effective

impedance of the free space,  $Z(\omega)$  is the relative impedance between the absorber and the free space. As shown in Fig. 4, the real part of the relative impedance of the metasurface structure is close to 1 in the frequency range from 1.25 to 3.5 THz while the image part is close to 0 in this band. This confirms that a good impedance matching between the air and metasurface structure is achieved resulting in a perfect absorption performance as shown in Fig. 1(b).

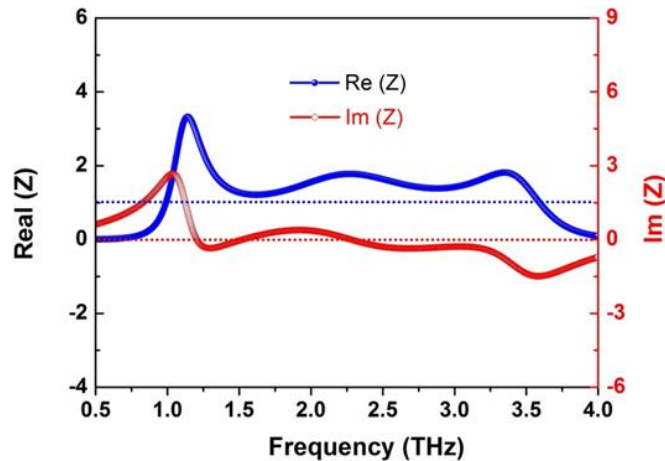


Figure 4. Relative impedance of the metasurface structure for metal phase of  $\text{VO}_2$  versus frequency.

To confirm the potential of the metasurface structure for practical applications, we investigate the absorption performance of the structure versus different incident angles under TE and TM polarizations. The absorption performance of the metasurface structure is realized in both the metal phase and dielectric phase of the  $\text{VO}_2$  layer. In the metal phase, in the TE polarization (Fig. 5(a)), the proposed metasurface structure works effectively with various values of incident angles under  $60^\circ$ . As the incident angle  $\theta$  increases, the absorption level is stable while the absorption bandwidth slightly moves to a higher frequency.

In the TM mode (Fig. 5(b)), the absorption level is also stable, but the absorption band significantly shrinks as  $\theta$  increases. It can be observed that when  $\theta$  is above  $40^\circ$ , two separate frequency bands show a strong absorption level. This means that the higher resonance of the metasurface structure moves significantly to a higher frequency band while the lower resonance does not change much. The distinction between the TE and TM modes may be explained by the fact that the absorption spectrum of the metasurface structure contains both magnetic and electric resonances [9]. In general, each of these two resonances responds differently to the incident angle. In the TE mode, for example, the magnetic resonant frequency is purely defined by geometric parameters and is unaffected by the incident angle, whereas its strength steadily decreases as the incident angle increases. Meanwhile, in the TM mode, the free electron density in the resistive pattern changes upon the change in the electric field at a certain incident angle, and strongly influences both magnetic and electric resonance frequencies [9].

Figs. 5(c) and (d) show the absorption performance of the metasurface structure in the dielectric phase of  $\text{VO}_2$ . It can be observed that the absorption level of the proposed structure is very weak at all of the incident angles and polarization angles. This result demonstrates that most incident EM waves are reflected and the metasurface structure is exhibited as a wideband reflector.

We also investigated the robustness of the proposed metasurface structure in the metal phase and dielectric phase of the  $\text{VO}_2$  layer under different values of polarization angle ( $\phi$ ) as shown in

Fig. 6. In this case, the incident wave was set perpendicular to the metasurface to observe the dependence of polarization angles.

When VO<sub>2</sub> is in the metal phase as can be seen from Fig. 6(a), the metasurface structure indicates a polarization-independent behavior, where the absorption and absorption bandwidth are nearly unchanged throughout the range of polarization angles from 0° to 90°. This result is straightforward due to the symmetry of the proposed structure.

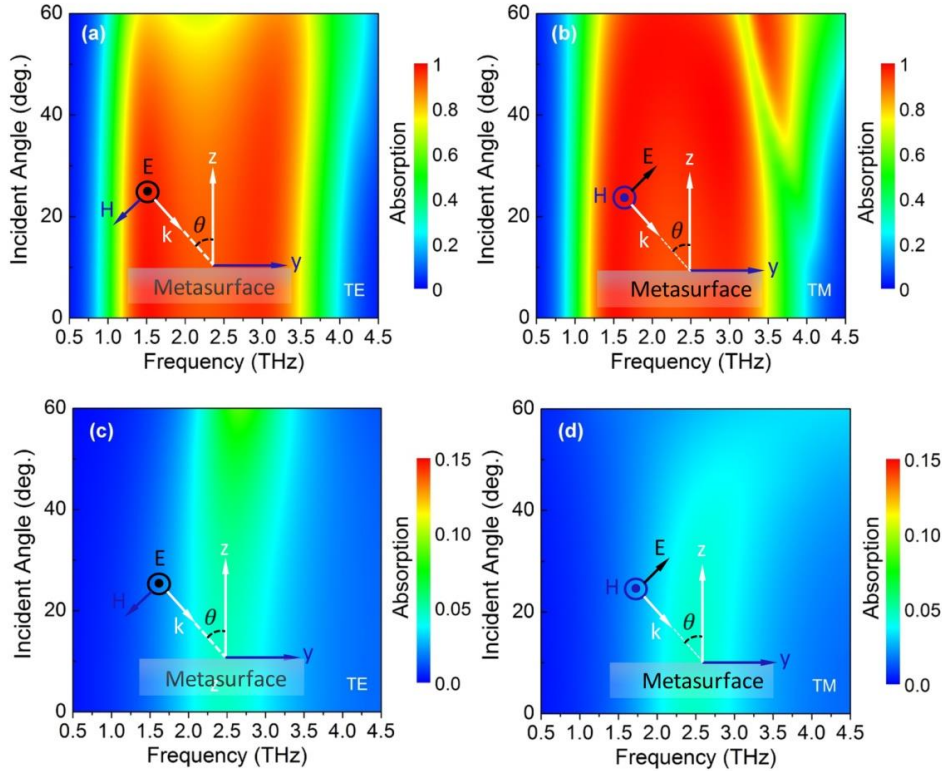


Figure 5. Absorption spectrum of the proposed metasurface structure versus incident angle for TE and TM polarizations: (a),(b) metalphase, and (c),(d) dielectric phase.

As shown in Fig. 6(b), when VO<sub>2</sub> turns to the dielectric phase, we can see that the absorption level of the metasurface structure is almost zero for any value of the polarization angle between 0° and 90°. This observation demonstrates that the metasurface structure acts as an insensitive-polarization THz wave reflector when VO<sub>2</sub> is in the dielectric phase.

The novelty and performance of the proposed bifunctional metasurface structure may be analyzed by comparison with some previous works on switchable/tunable THz absorbers as shown in Table 2. In this table, the absorption bandwidth includes operating band (in THz) and fractional bandwidth (in percent) which is defined as the ratio of the absolute bandwidth of absorption above 90 % to the central frequency of the absorption band. The incidence-insensitive angle is the maximum incident angle of the EM wave that the absorbance is still maintained above 80 % in the absorption bandwidth. Moreover, the number of layers of each structure is also taken to evaluate their fabrication difficulty. It can be seen from Table 2 that our design utilizes an easy-to-fabricate structure that also introduces the highest fractional bandwidth and a wide incidence-insensitive angle.

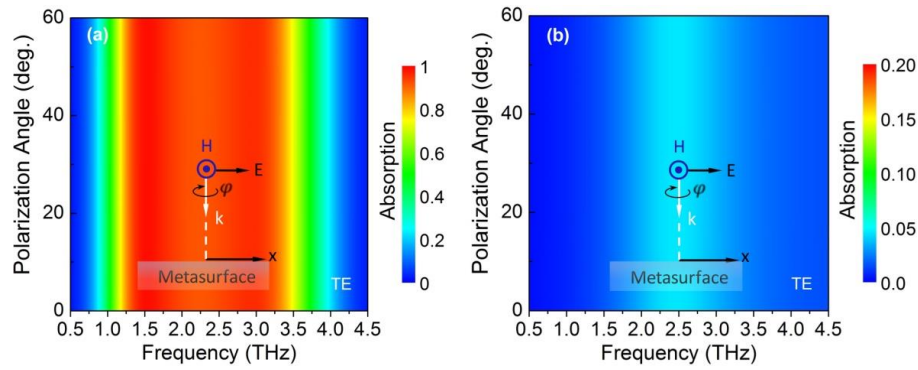


Figure 6. Absorption spectrum of proposed metasurface structure versus polarization angle in: (a) metal phase and (b) dielectric phase of the VO<sub>2</sub> layer.

Table 2. Performance comparison between the proposed structure with previous works.

Ref	Operating Band (THz)/ Fractional bandwidth (%)	Absorbance	Incidence-insensitive angle	Polarization-independent	Num. layers	Switchable material	Switchable method
10.	0.73 - 1.00 (30.8 %)	> 90 %	N/A	N/A	3	i-FLG	Optical
11.	1.18 - 1.64 (32.6 %)	> 90 %	60°	Yes	6	Graphene	Electrical
12.	1.50 - 2.75 (58.8 %)	> 90 %	70°	Yes	3	BDSs (AlCuFe)	Electrical
18.	0.74 - 1.62 (75.0 %)	> 90 %	55°	Yes	6	VO <sub>2</sub>	Thermal
19.	1.85 - 4.30 (79.7 %)	> 90 %	15°	Yes	3	VO <sub>2</sub>	Thermal
This work	1.29 - 3.26 (86.6 %)	> 90 %	60°	Yes	3	VO <sub>2</sub>	Thermal

#### 4. CONCLUSIONS

A high efficiency and wideband bifunctional metasurface structure operating as a nearly perfect absorber or reflector based on a phase-change material of vanadium dioxide (VO<sub>2</sub>) was proposed. The absorption and reflection of the metasurface structure were numerically investigated at different levels of the VO<sub>2</sub> conductivity. The results showed that in the metal phase of VO<sub>2</sub>, the metasurface structure exhibited a near-perfect absorber with an absorption of above 90 % in a wide frequency band from 1.29 THz to 3.26 THz. When VO<sub>2</sub> was in the dielectric phase, the proposed metasurface structure acted as a metallic mirror, reflecting all incoming THz waves in the frequency region. In addition, the proposed structure demonstrated that it could work effectively over a wide range of incident angles up to 60° and showed independent polarization behavior as well. The obtained results indicated that the proposed structure could be considered as a good candidate for bifunctional metasurface devices for THz applications.

**Acknowledgements.** This research is supported by the Ministry of Education and Training, Viet Nam (Grant No. B2021-TDV-05).

**CRedit authorship contribution statement.** N. T. Minh: Methodology, Investigation. N. T. K. Thu: Formal analysis, Funding acquisition. N. T. H. Van: Formal analysis, Investigation. N. T. M. Tam: Simulation, Validation. H. T. H. Thuong: Simulation, Validation. D. T. Phan: Investigation, Writing. V. D. Lam: Writing and editing. N. T. Q. Hoa: Conceptualization, Data curation, Writing and editing.

**Declaration of competing interest.** The authors declare that they have no known competing financial interests or personal relationships that could have appeared to influence the work reported in this paper.

## REFERENCES

1. Phare C., Daniel Lee Y. H., Cardenas J., and Lipson M. - Graphene electro-optic modulator with 30 GHz bandwidth, *Nat. Photon.* **9** (2015) 511-514. <https://doi.org/10.1038/nphoton.2015.122>.
2. Liu M., Yin X., Ulin-Avila E., Geng B., Zentgraf T., Ju L., Wang F., and Zhang X. - A graphene-based broadband optical modulator, *Nature* **474** (2011) 64. <https://doi.org/10.1038/nature10067>.
3. Kim I., Kim W. S., Kim K., Ansari M. A., Mehmood M. Q., Badloe T., Kim Y., Gwak J., Lee H., Kim Y. K., and Rho J. - Holographic metasurface gas sensors for instantaneous visual alarms, *Sci. Adv.* **7** (2021) eabe9943. <https://doi.org/10.1126/sciadv.abe9943>.
4. Lee D., Gwak J., Badloe T., Palomba S., and Rho J. - Metasurfaces-based imaging and applications: from miniaturized optical components to functional imaging platforms, *Nanoscale Adv.* **2** (2020) 605-625. <https://doi.org/10.1039/C9NA00751B>.
5. Liu M., Zhu W., Huo P., Feng L., Song M., Zhang C., Chen L., Lezec H. J., and Lu Y. - Multifunctional metasurfaces enabled by simultaneous and independent control of phase and amplitude for orthogonal polarization states, *Light Sci. Appl.* **10** (2021) 107. <https://doi.org/10.1038/s41377-021-00552-3>.
6. Song M., Wang D., Kudyshev Z., Xuan Y., Wang Z., Boltasseva A., Shalaev V. M., Kildishev A. V. - Enabling optical steganography, data storage, and encryption with plasmonic colors, *Laser Photon Rev.* **15** (2021) 2000343. <https://doi.org/10.1002/lpor.202000343>.
7. Ou J. Y., Plum E., Jiang L., and Zheludev N. I. - Reconfigurable photonic metamaterials, *Nano Lett.* **11** (2011) 2142. <https://doi.org/10.1021/nl200791r>.
8. Ou J. Y., Plum E., Zhang J., and Zheludev N. I. - An electromechanically reconfigurable plasmonic metamaterial operating in the near-infrared, *Nat. Nanotechnol.* **8** (2013) 252-255. <https://doi.org/10.1038/nnano.2013.25>.
9. Pham T. L., Xuan K. B., Tung B. S., Hai L. D., Long L. V., Lam V. D., and Tung N. T. - Origami-based stretchable bi-functional metamaterials: reflector and broadband absorber, *J. Phys. D Appl. Phys.* **54** (2021). <https://doi.org/10.1088/1361-6463/abdbe6>.
10. Masyukov M., Grebenchukow A. N., Livinov E. A., Baldycheva A., Vozianova A. V., and Khodzitsky M. K. - Photo-tunable terahertz absorber based on intercalated few-layer graphene, *J Opt.* **22** (2020) 095105. <https://doi.org/10.1088/2040-8986/abaa60>.
11. Mou N., Sun S., Dong H., Dong S., He Q., Zhou L., and Zhang L. - Hybridization-induced broadband terahertz wave absorption with graphene metasurfaces, *Opt. Express* **26** (2018) 11728-11736. <https://doi.org/10.1364/OE.26.011728>.
12. Jiang Y., Xinguo W., Wang J., and Wang J. - Tunable Terahertz absorber based on

- Bulk-Dirac-semimetal metasurface, *IEEE Photonics J.* **10** (2018) 4600607. <https://doi.org/10.1109/JPHOT.2018.2866281>
13. Song K., Wang K., Li J., and Liu Q. H. - Broadband tunable terahertz absorber based on vanadium dioxide metamaterials, *Opt. Express.* **26** (2018) 7148-7154. <https://doi.org/10.1364/OE.26.007148>
  14. Zhang H. T., Zhang L., Mukherjee D., *et al.* - Wafer-scale growth of VO<sub>2</sub> thin films using a combinatorial approach, *Nat. Commun.* **6** (2015) 8475. <https://doi.org/10.1038/ncomms9475>.
  15. Lei L., Lou F., Tao K., Huang H., Cheng X., and Xu P. - Tunable and scalable broadband metamaterial absorber involving VO<sub>2</sub> - based phase transition, *Photonics Res.* **7** (2019) 734-741. <https://doi.org/10.1364/PRJ.7.000734>.
  16. Liu M., Hwang H., Tao H., *et al.* Terahertz-field-induced insulator-to-metal transition in vanadium dioxide metamaterial, *Nature* **487** (2012) 345-348. <https://doi.org/10.1038/nature11231>.
  17. Chen J., Tang F., Wang X., Wu J., Wu Y., Ye X., Wang Y., and Yang L. - High efficiency broadband near-infrared absorbers based on tunable SiO<sub>2</sub>-VO<sub>2</sub>-MoS<sub>2</sub> multilayer metamaterials, *Results Phys.* **26** (2021) 104404. <https://doi.org/10.1016/j.rinp.2021.104404>.
  18. Yan D., Meng M., Li J., L. J., and Li X. - Vanadium dioxide-assisted broadband absorption and linear-to-circular polarization conversion based on a single metasurface design for the terahertz wave, *Opt. Express* **28** (2020) 29843. <https://doi.org/10.1364/OE.404829>.
  19. Huang J., Li J., Yang Y., Li, J., Li J., Zhang Y., and Yao J. - Broadband terahertz absorber with a flexible, reconfigurable performance based on hybrid-patterned vanadium dioxide metasurfaces, *Opt. Express* **28** (2020) 17832-17840. <https://doi.org/10.1364/OE.394359>.
  20. Tian J., Luo H., Yang Y., Ding F., Qu Y., Zhao D., Qiu M., and Bozhevolnyi S. I. - Active control of anapole states by structuring the phase-change alloy Ge<sub>2</sub>Sb<sub>2</sub>Te<sub>5</sub>, *Nat. Commun.* **10** (2019) 396. <https://doi.org/10.1038/s41467-018-08057-1>.
  21. Fang L. W. W., Zhao R., Li M., Lim K. G., Shi L., Chong T. C., and Yeo Y. C. - Dependence of the properties of phase change random access memory on nitrogen doping concentration in Ge<sub>2</sub>Sb<sub>2</sub>Te<sub>5</sub>, *J. Appl. Phys.* **107** (2010) 104506. <https://doi.org/10.1063/1.3383042>
  22. Gholipour B., Karvounis A., Yin J., Soci C., MacDonald K. F., and Zheludev N. I. - Phase-change-driven dielectric-plasmonic transitions in chalcogenide metasurfaces, *NPG Asia Mater.* **10** (2018) 533-539. <https://doi.org/10.1038/s41427-018-0043-4>.
  23. Mandal A., Cui Y., McRae L., and Gholipour B. - Reconfigurable chalcogenide phase change metamaterials: A materials, device and fabrication perspective, *JPhys. photonics* **3** (2021) 022005. <https://doi.org/10.1088/2515-7647/abe54d>.
  24. Galarreta C. R. de., Carrillo S. G. C., Au, Y. Y., Gemo E., Trimby L., Shields J., Humphreys E., Faneca J., Cai L., Baldycheva A. - Tunable optical metasurfaces enabled by chalcogenide phase-change materials: from the visible to the THz, *J. Opt.* **22** (2020) 114001. <https://doi.org/10.1088/2040-8986/abb5b>.